# PIC-MCC/Fluid Hybrid Model for Low Pressure Capacitively Coupled $O_2$ Plasma

Kallol Bera[a], Shahid Rauf[a] and Ken Collins[a]

[a]*Applied Materials, Inc.*
*974 E. Arques Ave., M/S 81517, Sunnyvale, CA 94085, USA*

**Abstract.** Low pressure capacitively coupled plasmas are extensively used for advanced microelectronic device fabrication. Due to long electron mean free path and large bias voltages in this regime, kinetic effects play an important role in the dynamics of low pressure discharges. To take account of the kinetic effects, a one-dimensional hybrid plasma model has been developed that couples the Particle-In-Cell (PIC) technique for charged species and a fluid method for neutral species. The PIC model uses the Monte Carlo Collision (MCC) method to account for collision processes. The fluid model for neutral species takes into account species transport in the plasma, chemical reactions, and surface processes. An electronegative $O_2$ plasma is simulated for a range of pressures (10-300 mTorr) and rf voltages (200-600 V) at 60 MHz. Our model for the $O_2$ plasma considers electrons, $O_2^+$, $O^-$, O, and O*. The reaction mechanism includes electron impact dissociation, ionization, dissociative attachment and ion-ion recombination. Computational results are compared to our previous simulations for an electropositive Ar discharge. The electrons primarily absorb power from the external power supply at the sheath edge during sheath expansion. Energetic beam electrons are generated at the sheath edge during electron heating, which are responsible for plasma production and sustenance through collisions. The negative ions are found to be confined in the bulk plasma due to the potential well. The ratio of negative ions to electrons increases with increase in pressure and decrease in rf voltage. The spatial profiles of charged and neutral species in the plasma are found to primarily depend on species sources due to collisional processes.

**Keywords:** PIC-MCC, hybrid model, capacitive plasma, electronegative, oxygen plasma.
**PACS:** 52.50.-b, 52.65.-y

## INTRODUCTION

Capacitively coupled plasma (CCP) discharges are widely used for plasma etching and deposition in the semiconductor industry. As feature sizes shrink in microelectronics devices, many plasma etching applications have transitioned to low pressures (< 30 mTorr) to reduce collision induced broadening of the ion angular distribution. Compared to medium/high pressure, CCP operation remains relatively less well-understood at low pressure as kinetic effects start playing an important role in the plasma dynamics. In the past, Turner and colleagues used Particle-In-Cell (PIC) models to illustrate electron heating mechanisms in low pressure CCPs [1,2]. Pressure effects and collisional drag forces on electrons were found to influence ohmic and non-collisional electron heating at the sheath edge. Kawamura *et al.* used a PIC-Monte Carlo Collision (MCC) model to investigate the dynamics of combined rf/dc sources [3]. Using PIC-MCC, Georgieva *et al.* showed that $CF_4$ plasma behaves like an electronegative discharge, and that $CF_3^+$ is the major positive ion [4]. Rauf *et al.* demonstrated that for an Ar plasma, the electrons absorb power at the sheath edge during sheath expansion, and the beam electrons are primarily responsible for plasma production and sustenance [5].

## COMPUTATIONAL MODEL

A 1D hybrid plasma simulation tool has been developed that couples a PIC model for charged species with a fluid model for neutral species at each time step. Our PIC model for charged species generally follows the methodology outlined in [6,7]. The PIC model includes Monte Carlo Collision (MCC) method to calculate collision

frequencies for various processes [8]. A database of collision cross-sections for various processes allows us to model both electropositive and electronegative plasmas [9]. The reaction mechanism includes electron impact dissociation, ionization, dissociative attachment and ion-ion recombination. Electron and ion momentum transfer collisions are also considered. The fluid model for neutral species takes into account species transport in the plasma, chemical reactions, and surface processes.

The program starts by initializing the location of all charged particles, velocities of all charged particles, and neutral species densities distribution. Probability arrays are set up for all particle collisions using the specified set of reaction cross-sections and initial species densities. When a particle of species $k$ collides with another species $j$ with density $n_j$ in reaction $j$, the collision frequency for this reaction is determined using

$$\nu_{k,i}(y,\varepsilon) = \sigma_i(\varepsilon) n_j(y) \sqrt{\frac{2\varepsilon}{m_k}} \tag{1}$$

where $\sigma_i$ is the collision cross-section for reaction $i$ and $m_k$ is mass of species $k$. $y$ is the distance from the ground electrode and $\varepsilon$ is the particle kinetic energy. Starting with the initial conditions, the electrode voltage is updated and particle positions are used to determine specie densities $n_k(y,t)$ for all charged species $k$, which are used to calculate the charge density $\rho(y,t)$. The Poisson equation is solved to compute the electrical potential, $\phi(y,t)$, that yields the electric field, $E(y,t)$. Using this electric field, all charged particles velocities are updated and the particles are moved. Particle velocity and location are staggered by half time-step and the leap-frog scheme is used for integrating the equations of motion [6]. The updated particle velocities and positions are used to gather statistics for the energy distribution functions. The power adsorbed by each particle $i$ of charged species $k$ is determined as

$$P_{i,k} = q_k \omega_k \, \mathrm{v}_{i,k} \, E(x_{i,k}) \tag{2}$$

where $\omega_k$ is the weight of the particle. The particle power absorption is then used to determine the spatial power distribution $P_k(y,t)$. Statistics of particles leaving the surfaces are collected and surface processes such as secondary electron emission are considered. Based on the probability arrays, particle collisions with each other and with the neutral fluid are considered. Statistics of these collisions are used to determine how electron energy is dissipated in the plasma, $P_{e\text{-}loss}$. Neutral species densities are calculated by solving the continuity equations for all neutral species.

## COMPUTATIONAL RESULTS

Simulations are performed for $O_2$ plasmas for 18,000 rf cycles at 60 MHz to ensure convergence of plasma properties. The inter-electrode gap is 0.05 m. The secondary electron emission coefficient is set to be 0.3. Results for statistical average of the last 36 cycles are reported. The simulation starts with 100000 particles and the time step for particle simulation is 50 ps. The $O_2$ plasma simulation results are compared with Ar plasma [5].

For the baseline condition of $O_2$ plasma at 200 V, 60 MHz, the simulation results for electric potential, electron, $O^-$ and $O_2^+$ densities are presented in Fig. 1 as a function of distance from the grounded electrode ($y$) and phase during one rf cycle. The rf voltage is applied to the right electrode. The positive ions ($O_2^+$) are formed through ionization and negative ions ($O^-$) by electron attachment. During the first half of the rf cycle, the applied voltage is positive, and this voltage primarily drops at the left electrode. The sheath collapses at the right electrode, and electrons are pulled to the right electrode. The situation reverses in the second half of the rf cycle. Both positive and negative ions have large masses, and their densities do not change significantly during the rf cycle.

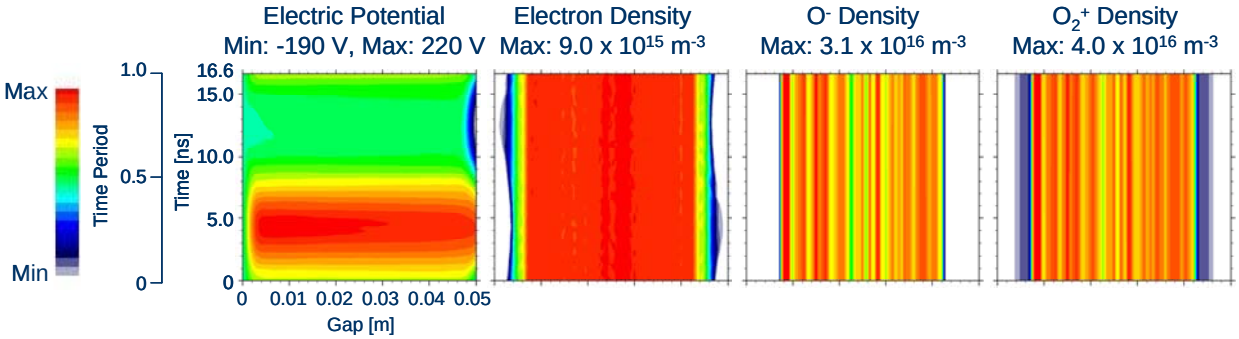


**FIGURE 1.** Electrical potential, and electron, $O^-$ and $O_2^+$ densities at 20 mT, 200V, 60 MHz

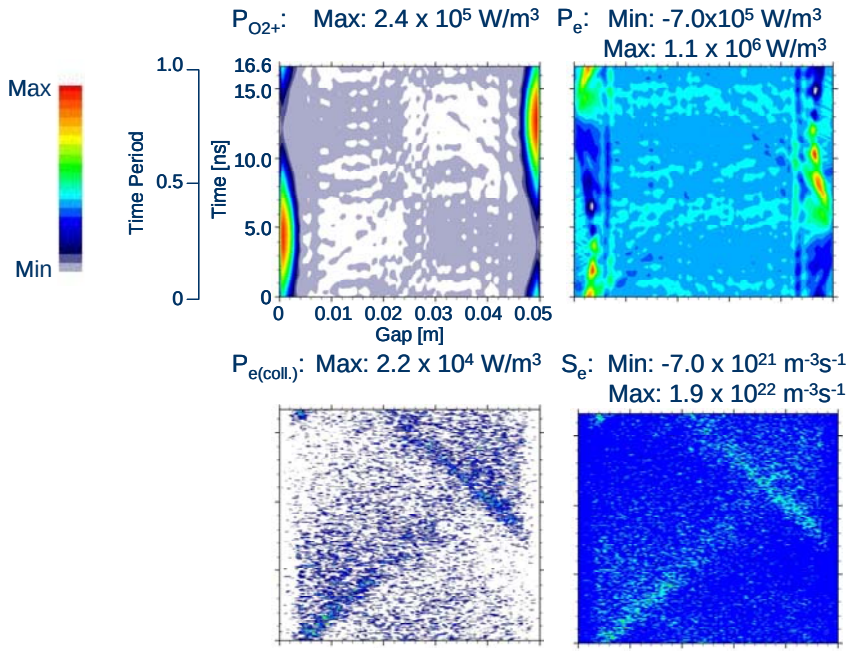


**FIGURE 2.** $O_2^+$, electron and $O^-$ power deposition, electron energy loss and electron source at 20 mT, 200V, 60 MHz

The $O^-$ density is confined in the bulk plasma due to the potential well, and has a peak near the center of the discharge. Because the $O^-$ density is larger than the electron density, the $O_2$ plasma is highly electronegative. To maintain charge neutrality in the bulk region, the $O_2^+$ density is the sum of electron and $O^-$ densities. The peak electron density for Ar plasma under the same condition is 1.61 x $10^{16}$ m$^{-3}$ [5]. The electron density is lower for the $O_2$ plasma as some electron energy is used for dissociation and electrons are lost due to attachment.

The power absorbed by $O_2^+$ ions and electrons from electric field, power lost by electrons during collision and electron source due to ionization are shown in Fig. 2. The plasma potential being positive compared to the electrodes, positive ions gain energy during acceleration to the electrodes. The electrons gain energy from the electric field at the sheath edge when the sheath expands into the plasma, and pushes electrons into the bulk plasma. When the sheath contracts, electrons return some of the power back to the electric field, and decelerate in the sheath. The $O^-$ power deposition is much smaller than the electron power deposition. The electron gains energy during sheath expansion and the energetic beam electrons shoot into the bulk plasma. The beam electrons travel considerable distance into the bulk, and dissipate their energy through collisions. Apart from beam electrons, the secondary electrons emerging from the electrodes due to ion bombardment carry energy that is dissipated in the bulk plasma. Most of the energy lost by the electrons is through ionization and dissociation of $O_2$. There is also small amount of energy lost due to excitation of O. These inelastic processes occur mainly due to high energy beam electrons. The electron energy loss in elastic collision is small and spreads over the discharge region.

## Pressure Effect

The effect of pressure on electron density is shown in Fig. 3 for the $O_2$ plasma at 200 V and 60 MHz. For a constant rf voltage, the electron density increases with pressure as neutral density increases, which is similar to what was observed in Ar plasma [5]. The sheath thickness decreases as the electron density increases. The peak electron power deposition increases from 3.2 x $10^5$ W/m$^3$ at 10 mT to 2.4 x $10^6$ W/m$^3$ at 300 mT. As shown in Fig. 4, the negative ion density increases with pressure due to more electron attachment at higher neutral density. The ratio of $O^-$ ions to electrons increases with pressure in general as electron attachment increases faster than electron impact ionization. However, at the very low pressure of 10 mT, energetic electrons reach the opposite electrode, reducing electron generation through ionization, and therefore the electron density.

Electron power loss during collision is shown in Fig. 5 for gas pressure ranging 10 to 300 mT. The beam electrons are stronger at lower pressure, and retain their beam character for a long distance even after beam electrons

are launched from the other sheath. At 10 mT, the beam electrons entering the opposite sheath during sheath contraction cause ripples as shown in Fig. 3. At higher pressures, the beam electrons originating from one sheath stop before the beam electrons are launched from the opposite sheath.

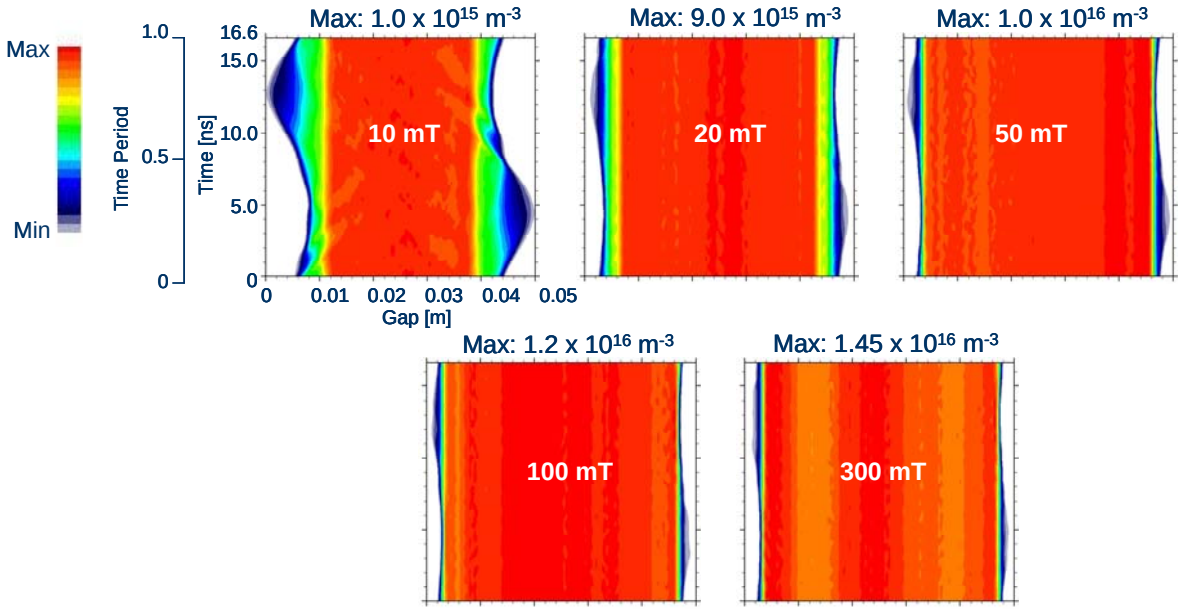


**FIGURE 3.** Electron density at different pressures (10-300mT) at 200V, 60 MHz

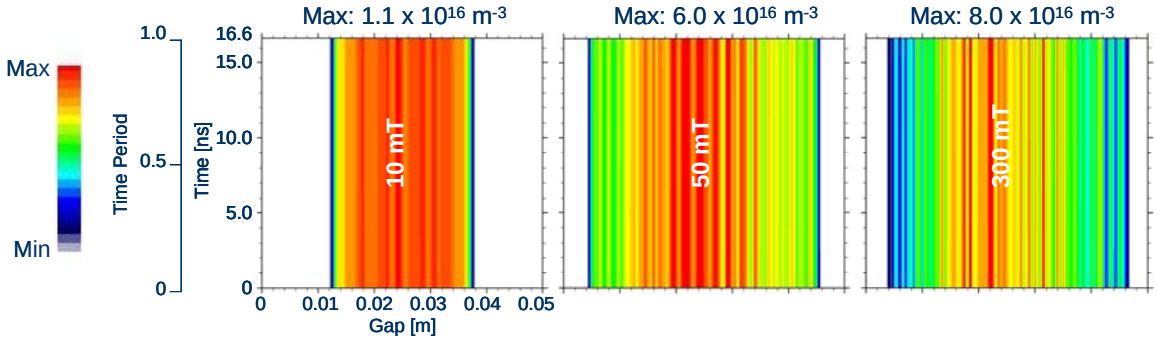


**FIGURE 4.** O- density at different pressures (10-300 mT) at 200V, 60 MHz

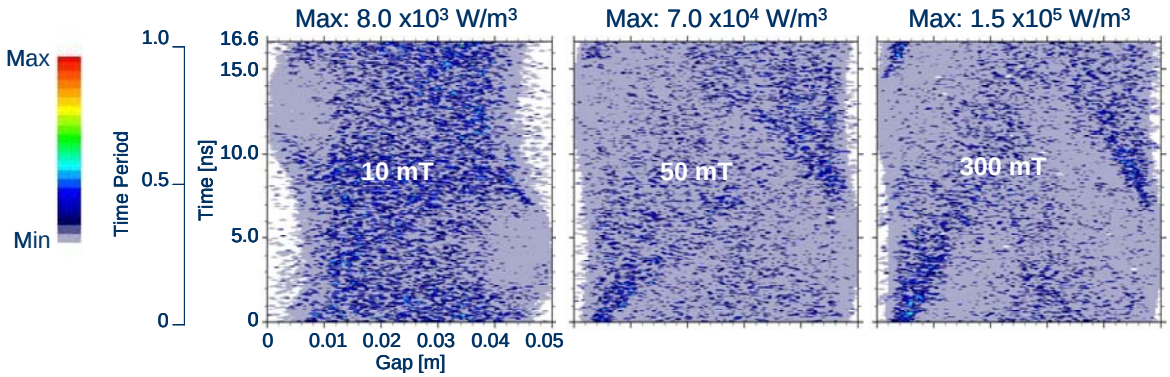


**FIGURE 5.** Electron energy loss at different pressures (10-300mT) at 200V, 60 MHz

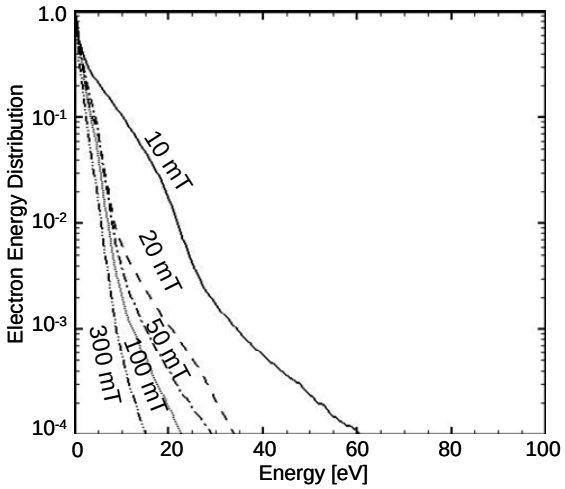


**FIGURE 6.** Electron energy distribution at different pressures (10-300mT) at 200V, 60 MHz

The electron energy distribution (EED) in the bulk plasma is shown in Fig. 6 at different pressures. At higher pressure, the electron temperature is lower compared to that that at lower pressure. Lower temperature reduces ionization, diminishing the effectiveness in increase in electron density due to higher neutral density as shown in Fig. 3. Negative ions also play a role in determining the electron density at different pressures. At 10 mT, the electron energy is enhanced near 20 eV. This is due to beam electrons that reach further into the bulk plasma. As the beam electron effect diminishes at higher pressure, this peak in EED reduces.

## Voltage Effect

The effect of rf voltage on the electron density is shown in Fig. 7 for the $O_2$ plasma at 10 mT and 60 MHz. The electrons are more energetic at higher rf voltage leading to better ionization. The electron source in the plasma due to ionization increases. The electron density increases, and sheath thickness decreases. Also, the ratio of $O^-$ ions to electrons decreases. The peak electron power deposition increases from 3.2 x $10^5$ W/m$^3$ at 200 V to 2.1 x $10^6$ W/m$^3$ at 600 V. At higher voltage, the beam electrons penetrate further into the bulk plasma leading to higher collisional loss in the bulk plasma as shown in Fig. 8. The electron energy distribution (not shown) exhibits energy enhancement near 20 eV at 600 V due to the beam electrons.

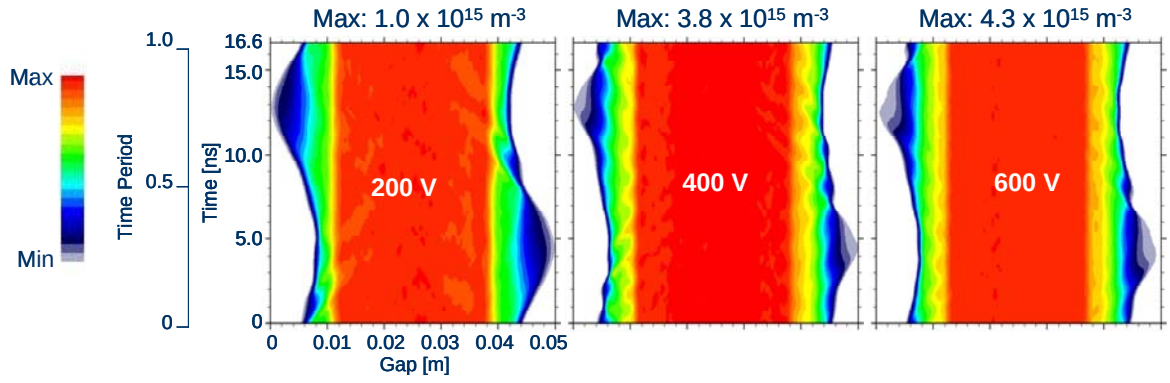


**FIGURE 7.** Electron density at different voltages (200-600 V) at 10 mT, 60 MHz

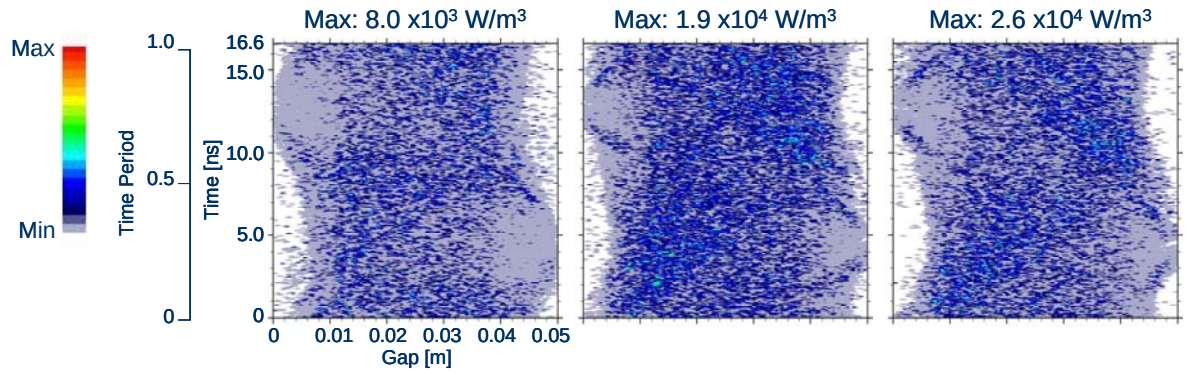


**FIGURE 8.** Electron energy loss at different voltages (200-600 V) at 10 mT, 60 MHz

## CONCLUSIONS

For low pressure rf capacitively coupled plasmas, the electrons primarily absorb power from the sheath edge during sheath expansion. The energetic beam electrons, generated at the sheath edge during electron heating, are responsible for plasma production and sustenance through collisions. For an $O_2$ plasma, the electron density is lower compared to an Ar plasma due to the dissociation and attachment processes. The ratio of $O^-$ ion to electron density increases with an increase in pressure, and a decrease in rf voltage where effectiveness of the beam electrons diminishes.

## REFERENCES


1. M. M. Turner and M. B. Hopkins, *Phys. Rev. Lett.*, **69**, 3511-3514 (1992).
2. M. M. Turner, *Phys. Rev. Lett.*, **75**, 1312-1315 (1995).
3. E. Kawamura, M. A. Lieberman, A. J. Lichtenberg and E. A. Hudson, *J. Vac. Sci. Technol.* **A 25**, 1456 (2007).
4. V. Georgieva, A. Bogaerts and R. Gijbels, *J. Appl. Phys.*, 93, 2369-2379 (2003).
5. S. Rauf, K. Bera and K. Collins, *Plasma Sources Sci. Technol.*, **19**, 015014 (2010).
6. C.K. Birdsall and A.B. Langdon, *Plasma Physics via Computer Simulation*, Bristol: Institute of Physics, 1991.
7. W.S. Lawson, *J. Comput. Phys.*, **80**, 253-276 (1989).
8. V. Vahedi and M. Surendra, *Comput. Phys. Commun.*, **87**, 179-198 (1995).
9. S. Rauf and M.J. Kushner, *J. Appl. Phys.*, **82**, 2805-2813 (1997).